Spatial Evolution of Wave-Particle Interaction Region Deduced From Flash-Type Auroras and Chorus-Ray Tracing

Mitsunori Ozaki[1] [ID], **Tomohiro Inoue[1], Yoshimasa Tanaka[2]** [ID], **Satoshi Yagitani[1]** [ID], **Yoshiya Kasahara[1]** [ID], **Kazuo Shiokawa[3]** [ID], **Yoshizumi Miyoshi[3]** [ID], **Kousuke Imamura[1]** [ID], **Keisuke Hosokawa[4]** [ID], **Shin-ichiro Oyama[2,3,5]** [ID], **Ryuho Kataoka[2]** [ID], **Yusuke Ebihara[5]** [ID], **Yasunobu Ogawa[2]** [ID], and **Akira Kadokura[2]** [ID]

[1]Graduate School of Natural Science and Technology, Kanazawa University, Kanazawa, Japan, [2]National Institute of Polar Research, Tachikawa, Japan, [3]Institute for Space-Earth Environmental Research, Nagoya University, Nagoya, Japan, [4]The University of Electro-Communications, Chofu, Japan, [5]Research Institute for Sustainable Humanosphere, Kyoto University, Uji, Japan

Abstract In-situ observations of spatial variations of the wave-particle interaction region require a large number of satellite probes. As an alternative, flash-type auroras, a kind of pulsating aurora, driven by discrete chorus elements, can be used to investigate the interaction region with a high spatial resolution. We estimated the spatial extent of wave-particle interaction region from ground-based observations of flash aurora at Gakona (62.39°N, 214.78°E), Alaska at subauroral latitudes, and found that the auroral expansion was predominantly to the low-latitude side. The spatial displacement is thought to be caused by the propagation effects of chorus waves in the magnetosphere. Using ray tracing analysis to take into account chorus wave propagation, we reconstructed the spatiotemporal evolution of the volume emission rate and confirmed that the predominant expansion is toward the lower-latitude side in the ionosphere. This study shows that chorus wave propagation in the magnetosphere gives new insight for characterizing the transverse size (across the geomagnetic field line) of wave-particle interaction regions. The calculated spatial scale of the column auroral emission shows a correlation with the magnetic latitude of the resonance region at magnetic latitudes within 10° of the equatorial plane of the magnetosphere. Our results suggest that the spatial scale of a flash aurora is indirectly related to the chorus amplitude because the latitudinal range of the wave-particle interaction is important for the growth of wave amplitude.

1. Introduction

Cyclotron resonant wave-particle interactions are of fundamental importance as ubiquitous drivers of particle heating, acceleration, and precipitation throughout supernova remnants (Malkov et al., 2011), magnetized planets (Treumann, 2006), comets (Sagdeev et al., 1986), and shocks (Winske & Leroy, 1984) in space plasma physics and astrophysics. Chorus waves, which are coherent electromagnetic emissions commonly generated in Earth's magnetosphere (Burton & Holzer, 1974; Li et al., 2009; Tsurutani & Smith, 1974) and magnetized planets (Coroniti et al., 1980; Kurth & Gurnett, 1991; Menietti et al., 2013), have a crucial role in energetic particle dynamics in the radiation belts via wave-particle interactions (Bingham et al., 2018; Horne et al., 2003; Li et al., 2014; Miyoshi et al., 2003, 2013; Omura et al., 2007; Summers et al., 1998; Thorne et al., 2013). A single chorus element can effectively accelerate electrons to relativistic energies (Foster et al., 2017). Additionally, a single chorus wave packet can rapidly and effectively scatter energetic electrons into the atmosphere, illuminating flash-type auroras (Ozaki et al., 2019) and microbursts (Breneman et al., 2017; Lorentzen et al., 2001; Mozer et al., 2018; Rosenberg et al., 1981) as a signature of the wave-particle interaction region. The spatial scales of chorus element wave-particle interactions have been estimated based on multiple satellite observations of chorus elements (Agapitov et al., 2010, 2017; Santolík & Gurnett, 2003; Shen et al., 2019; Turner et al., 2017). The transverse scales across the geomagnetic field line of a coherent chorus source range from tens to thousands of kilometers. The statistical results of multiple satellite observations of discrete chorus elements in the lower band indicate that the transverse scales of a chorus source increase with higher L shells and higher magnetic latitudes (Shen et al., 2019). Such

dependence of the spatial scale can be used to predict the effects of chorus wave propagation in the magnetosphere from the wave-particle interaction region.

Although multiple satellite observations have been well studied providing static snapshots of wave-particle interaction regions, the quantitative spatiotemporal development in the transverse direction of the background field line requires further study. In this study, we overcome the difficulty of transient spatial perception of wave-particle interaction regions by using flash aurora images in the ionosphere. Moreover, we analyze the effects of chorus wave propagation on spatial development by calculating the volume emission rate (VER) at the ionospheric footprints connected to the chorus ray paths using ray tracing analysis (e.g., Kimura et al., 1985). Quantifying the prompt responses of the spatial development of the wave-particle interaction region is essential for quantitative radiation belt models (Jordanova et al., 2016; Ma et al., 2018; Omura et al., 2015; Seki et al., 2018; Soria-Santacruz Pich et al., 2017). It also contributes to the understanding of the largest contribution to the loss of plasma sheet electrons into the atmosphere (Ni et al., 2008; Thorne et al., 2010; Miyoshi, Oyama, et al., 2015, Miyoshi, Saito, et al., 2015, Miyoshi, et al., 2020).

2. Flash-Type Auroral Observations

Pulsating auroras have been categorized into several types according to their spatiotemporal characteristics (Oguchi, 1978; Nishimura et al., 2020 and references therein). Flash-type auroras are related to pulsating aurora as both are the luminous phenomena driven by chorus waves. A flash aurora is a transient (<hundreds of milliseconds) optical emission in the upper atmosphere, so a typical ground-based network of auroral cameras, such as THEMIS (Time History of Events and Macroscale Interactions during Substorms) ASI (Donovan et al., 2006), OMTIs (Optical Mesosphere Thermosphere Imagers) (Shiokawa et al., 1999), or the WMI (Watec monochromatic imager) system (Ogawa et al., 2020), with a sampling rate on the order of seconds cannot detect such short visible bursts. Flash auroras show a drastic shorten duration (less than 0.5 s) than typical pulsating auroras and are driven by a pure single discrete chorus element. Flash auroras show a patchy type of spatial development and are a useful ionospheric screen of wave-particle interaction region in the magnetosphere (Ozaki et al., 2019). It is noteworthy here that Kataoka et al. (2012) reported very rapid pulsating auroras exceeding an order of magnitude higher than 3 Hz modulation of pulsating auroras, which is repetitive and associated with standard pulsating auroras. Such rapid luminous modulations of pulsating auroras showing repetitive luminous modulations can be different from the transient appearance of flash auroras.

Here, we focus on flash auroras to evaluate the spatial evolution of interaction regions between a pure single chorus element and energetic electrons. Statistical spatiotemporal characteristics of flash auroras remain poorly understood owing to the difficulty in long-term setup of optical observation with a high-temporal resolution beyond a 30-frames-per-second rate. We used recent high-speed EMCCD (electron multiplying charge coupled device) camera observations for the ERG-ground coordinated network. One of the EMCCD cameras operated by PWING (the study of dynamical variation of Particles and Waves in the INner magnetosphere using Ground-based network observations) (Shiokawa et al., 2017) has been placed at Gakona (62.39°N, 214.78°E), Alaska, since 2017. In the present study, approximately 100 flash aurora events recorded at 100 frames per second were identified between 13:00 and 13:30 UT (morning sector in MLT), March 30, 2017. The EMCCD images were taken through an RG665 long-pass filter, which has a cutoff frequency of 665 nm. The nitrogen first positive bands can be major emissions in the pass band (Chamberlain, 1961). The period of data analysis includes the case study of discrete chorus elements by the Arase satellite and flash auroras at the magnetic conjugate ground station by Ozaki et al. (2019).

Raw (256 × 256 pixels) images of flash auroras by the EMCCD all-sky camera were converted to images in the local East, North, UP (ENU) Cartesian coordinate system under an assumption that the altitude is 110 km. The spatial resolution of the images in ENU coordinates is 3 × 3 km. Each pixel value was high-pass filtered with a cut-off frequency of 0.05 Hz to mitigate the effects of stray light. A median filter for the images' squared pixel values was used with a 15 × 15-km block to remove impulse noise. The duration of an auroral emission was extracted from 100-Hz images, and the spatial scale of an auroral patch was extracted using Otsu's method (Otsu, 1979) from 25-Hz images to improve the signal-to-noise ratio. Otsu's method is
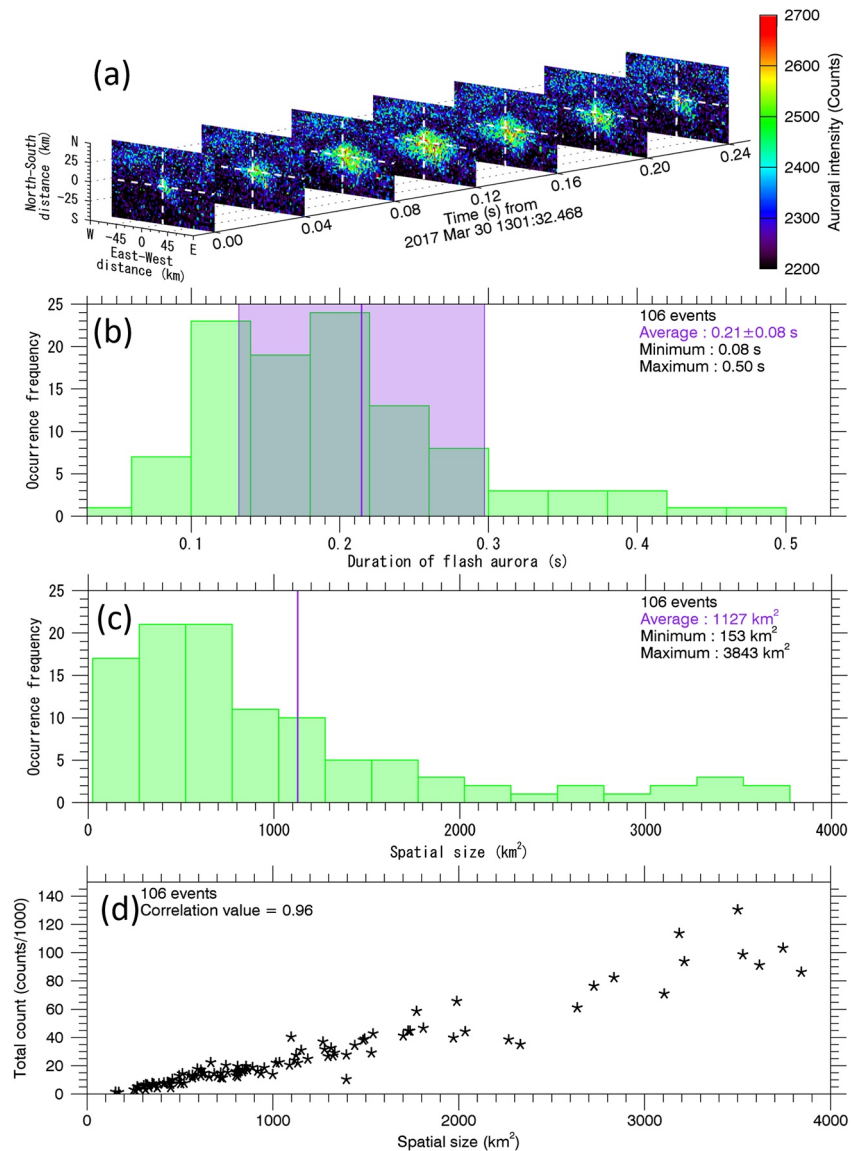
Figure 1. (a) Sequence snapshots of an example of a flash aurora observed with the electron multiplying charge coupled device all-sky camera at Gakona showing expansion and contraction. Histograms of (b) the luminous duration and (c) the maximum spatial size of flash auroras in the ionosphere (110 km). The solid purple lines indicate the average value and the purple rectangle indicates the standard deviation. (d) Correlation between spatial size of flash aurora and total counts in the maximum auroral patch.

a typical automatic segmentation technique that finds an optimal threshold based on a histogram of pixel values.

3. Observation Results

Figure 1a shows a typical example of sequential snapshots of a flash aurora observed with the EMCCD all-sky camera at Gakona that exhibits a spatial displacement (for this example, from north to south). Spatiotemporal imaging of flash auroras provides spatial characteristics (size and evolution) of source regions of chorus element wave-particle interactions through its high spatial resolution compared with those obtained from in situ observations of discrete chorus elements. The luminous duration and the maximum spatial size of a single flash aurora in the ionosphere (110 km) are plotted in Figure 1b and 1c, respectively. The average luminous duration is 0.21 ± 0.08 s, which applies to 70% of all flash auroras. This average
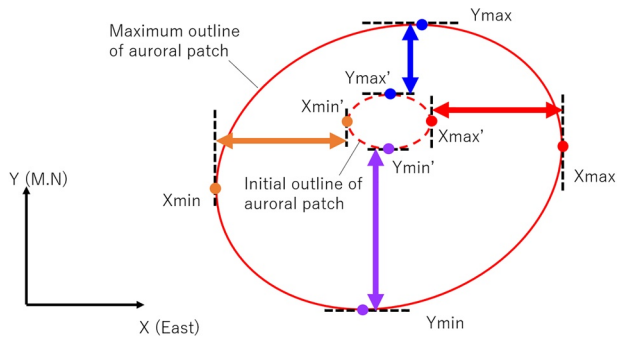
Figure 2. Schematic diagram of spatial displacement of an aurora patch in East, North, UP coordinates. The positive y and x directions are the magnetic north and east directions, respectively.

luminous duration is comparable with the duration of discrete chorus elements (Teng et al., 2017) supporting the proposition that flash auroras indicate the source region of chorus element wave-particle interactions. For all events, the maximum size of flash auroras across the geomagnetic field line varies from 153 to 3,843 km^2, with the average size of 1,127 km^2. For the wide spatial range of auroral observations, flash auroras with a larger auroral size showed a longer luminous duration, but neither the histogram for the luminous duration nor that for auroral size showed a correlation with the magnetic latitudes and longitudes in the field of view of the all-sky images. In contrast, the statistical results of the observed auroral sizes reveal that there is a significant positive correlation between total counts integrating within a flash auroral region and auroral size, as shown in Figure 1d. The flash auroral intensity is calculated by subtracting the background counts from raw count images just before the initial light emission to mitigate the effects of background diffuse auroras and stray light. The auroral intensity was concentratively distributed in a narrow range from 2,400 to 2,600 counts at each pixel in the auroral area, and thus we found a significant correlation ($r = 0.96$) between the total counts within a flash auroral region and auroral size. Raw count values at each pixel can be related to precipitating energetic electron fluxes connected to each geomagnetic field line. This clear positive correlation indicates that there is a limit imposed on precipitating energetic electron fluxes by chorus element wave-particle interactions, similar to that imposed on trapped electron fluxes in the inner magnetosphere by chorus wave-particle interactions (Kennel & Petschek, 1966). The pitch angle diffusion is related to chorus wave amplitude (Albert, 2005; Li et al., 2013; Tao et al., 2012) and chorus waves show saturation in the amplitude of the wave packet (Santolík et al., 2003; Summers et al., 2012). If the scattering rate inside the interaction region of the flash aurora does not reach the diffusion limit, each pixel can take various count values depending on the precipitating electron flux within flash auroral patches. Then, the observed correlation between auroral size and total counts within the auroral patch would be low. Kasahara et al. (2019) reported that the full filling of the loss cones of energetic electrons associated with chorus waves is commonly seen in in-situ observations. Thus, the positive correlation suggests that the chorus wave growth saturates and/or reaches a strong diffusion limit due to the intense amplitude (Kennel, 1969). The plateau of pitch angle diffusion coefficient for a larger chorus amplitude (e.g., see Figure 2 in Tao et al., 2012) results from the wave-particle interactions.

Next, the spatial displacement was estimated by subtracting the maximum outline of the flash aurora from the initial outline. The red dash in Figure 2 indicates each coordinate value for the initial outline of an auroral patch. The spatial displacement in each direction at the ionospheric altitude was calculated by subtracting the maximum outline (red solid) of the flash aurora from the initial outline (red dash), as shown in Figure 2. The northward and southward expansions were calculated as $\left(y_{\max} - y'_{\max}\right)$ and $\left(y_{\min} - y'_{\min}\right)$, respectively. The eastward and westward expansions were calculated as $\left(x_{\max} - x'_{\max}\right)$ and $\left(x_{\min} - x'_{\min}\right)$, respectively. Here, $y_{\max}$ $\left(x_{\max}\right)$ and $y_{\min}$ $\left(x_{\min}\right)$ are the maximum and minimum coordinate $y(x)$ values of the maximum outline of an auroral patch in ENU coordinates, respectively.

Figure 3 shows the spatial displacements of flash auroras in the magnetic north to south and east to west directions at an ionospheric altitude of 110 km. Consistent with the study of Ozaki et al. (2019), most events of the flash auroras show significant asymmetric spatial developments in the magnetic north to south direction, but no significant asymmetric spatial developments in the east to west direction. 17% (2%) of the flash auroral events exhibit southward (northward) expansion over 10 km. As shown in Figure 1d, the southward expansion makes an important contribution to the increase in total counts in the maximum auroral patch because expansion increases the total area of the auroral patch. The average southward displacement of 6.96 km in Figure 3b is 2.4 times larger than the average northward displacement of 2.86 km in Figure 3a in the ionosphere. Such spatial dependence would imply that if these flash auroras are generated by wave-particle interactions with individual chorus elements, then the wave-particle interaction regions in the magnetosphere have a preferential earthward spatial development as a common feature, which has not been identified by multiple satellite observations of chorus elements.
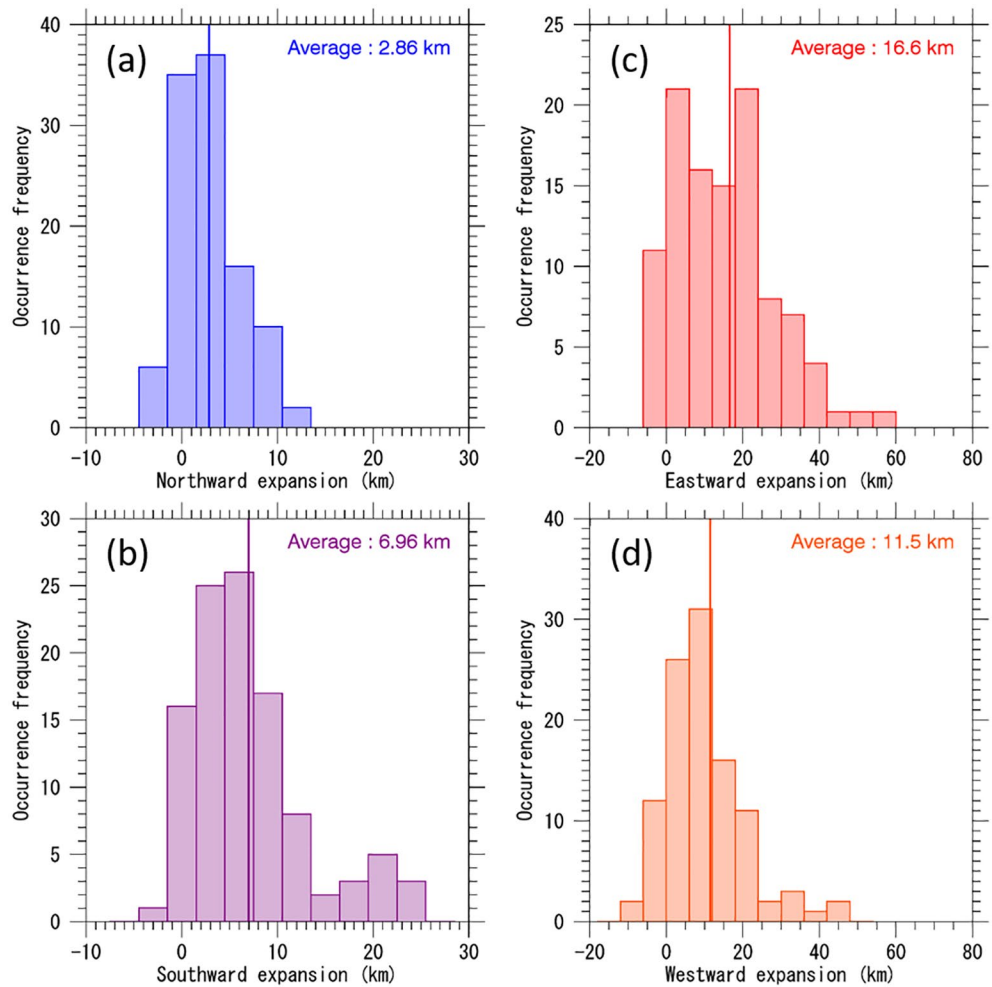
Figure 3. Histograms of (a) northward, (b) southward, (c) eastward, and (d) westward expansion of flash auroras. The solid lines indicate the average value.

Table 1
Calculation Parameters

Parameters	Value	Unit
Wave frequency	0.2–0.5	fce
Frequency resolution	0.01	fce
Sweep rate of chorus element	5.0	kHz/s
Duration of chorus element	0.264	s
Width of WNA	25	deg.
Resolution of WNA	5.0	deg.
Distance resolution of ray tracing	10	km
Angle resolution of ray tracing	1.0	deg.
Initial source location in SM coordinates	$(-4.46, -2.87, 0.04)$	Re
Energy range	0.3 to 50	keV
Energy resolution	50	eV

Abbreviations: SM, solar magnetic; WNA, wave normal angle.

4. Effects of Chorus Wave Propagation

The observed spatial characteristics of flash auroras could result from propagation of chorus waves from the equator to higher magnetic latitudes. The propagation effects of chorus wave in the nonducted mode are evaluated using ray tracing analysis for the spatial development of flash auroras. We use the global core plasma model (GCPM 2.2) (Gallagher et al., 2000) for the cold electron density and the Tsyganenko 2002 model (Tsyganenko, 2002) for the geomagnetic field lines. The calculation parameters are listed in Table 1. A chorus source is assumed to be a point source (see Figure 4a) because the Larmor radii of energetic (tens of keV) electrons as seed particles are less than 10 km, which is smaller than the spatial mesh size in the ray tracing. South-bound chorus rays are launched with up to an initial wave normal angle (WNA) of 25° from the magnetic equator and a radial distance of 5.3 Re (outside of plasmapause) in solar magnetic (SM) coordinates, where Re is the Earth's radius. As shown in Figure 4b, the frequency sweep rate of a rising tone element is assumed to be 5.0 kHz/s. The frequency range is from 0.2 to 0.5 fce, where
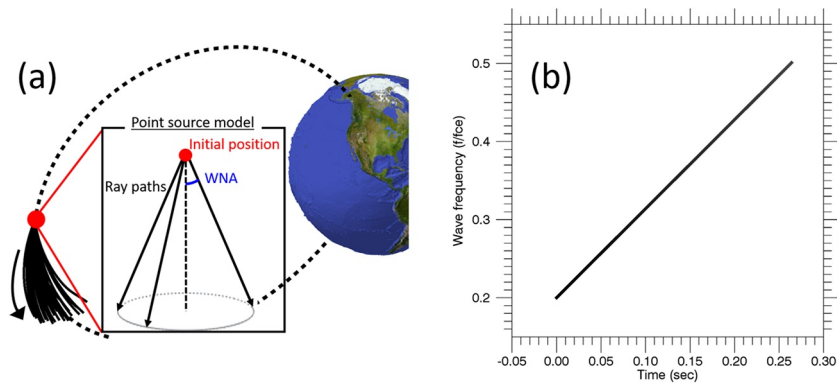
Figure 4. Calculation model of chorus-ray tracing. (a) A point source is located at the magnetic equator, and the wave normal angle of chorus rays is based on the magnetic field line connected to the point source. (b) Model of discrete element of lower-band chorus.

fce is the electron gyrofrequency at the equator under the assumption of the typical lower-band chorus. The duration of a chorus element is therefore 0.264 s.

The VER in the ionosphere was calculated using the following steps. First, numerous chorus-ray paths with different wave normal angles and frequencies were calculated with the GCPM 2.2 model and the Tsyganenko 2002 model. The resonance energy for each chorus-ray path in the magnetosphere was calculated. When energetic electrons satisfy the first-order resonance condition with chorus rays given in equation (2) in a reference of Bortnik et al. (2006), the resonance locations in the magnetosphere are projected to the ionosphere with the travel time along the geomagnetic field line. The ionospheric footprints were calculated by tracing magnetic field lines from each resonance location with the Tsyganenko 2002 model. Then, the travel time of resonant particles was calculated from the resonance location to the ionospheric footprint at the altitude of 110 km. Then, the VER in the ionosphere for the nitrogen first positive band of 670.5 nm is calculated based on a method proposed by Ono (1993). The time constant for the 670.5 nm emission is microseconds and there are no afterglow effects like slow optical emissions for 557.7 and 630.0 nm wavelengths (Hanna & Anger, 1971). The precipitating electrons are assumed to consist of superposed narrow Gaussian distributions $j_0 \exp\left(-\left(E - E_0\right)^2 / W^2\right)$, where j_0 is the maximum flux at the resonance location from the AE9 model (Ginet et al., 2013), E is the kinetic electron energy, E_0 is the characteristic energy, and W is the energy width, which equals $0.25E_0$. The energy width is the same as that estimated in Ono (1993) to be the characteristic energy of pulsating aurora. The characteristic energy is simply assumed to be the resonance energy of energetic electrons that interact with chorus rays. The parameters in all models were determined at the time of the optical observation on March 30, 2017 ($Kp = 3$). Finally, the column emission was calculated by integrating the VER along the line of sight in the altitude range from 80 to 300 km. The effects of pitch angle change of energetic electrons are not taken into account in this VER calculation. Our simple model is considered to be appropriate because although the pitch angle change is important for a rigorous evaluation of the luminous value in an auroral patch, it is not essential for the estimation of the spatial characteristics of flash auroral size.

Figure 5a shows the electron density profile in SM coordinates. The red dot is a source point of chorus rays. The dotted lines indicate field lines for L-values of 2, 3, 4, 5, and 6, respectively. Figure 5b shows the different frequency chorus rays spreading only from initially perfect parallel propagation at the equator in the XZ plane of SM coordinates. Figure 5c and 5d show the resonance energy and the travel time of resonant electrons that interact with the chorus rays at the various locations. The travel time is calculated along the trajectory from the interaction region to the ionosphere in the opposite hemisphere (at an altitude of 110 km). The chorus propagation is simulated up to the magnetic latitude of 10°. As shown in Figure 5, the chorus rays interacting with energetic (tens of keV) electrons deviate radially inward from the magnetic field line connected to the point source. The propagation characteristics are similar to those reported in previous studies (Chen et al., 2013; Chum & Santolík, 2005). The inward wave propagation is dominant over the outward wave propagation from the source location of chorus elements that are resonant with 10 s of
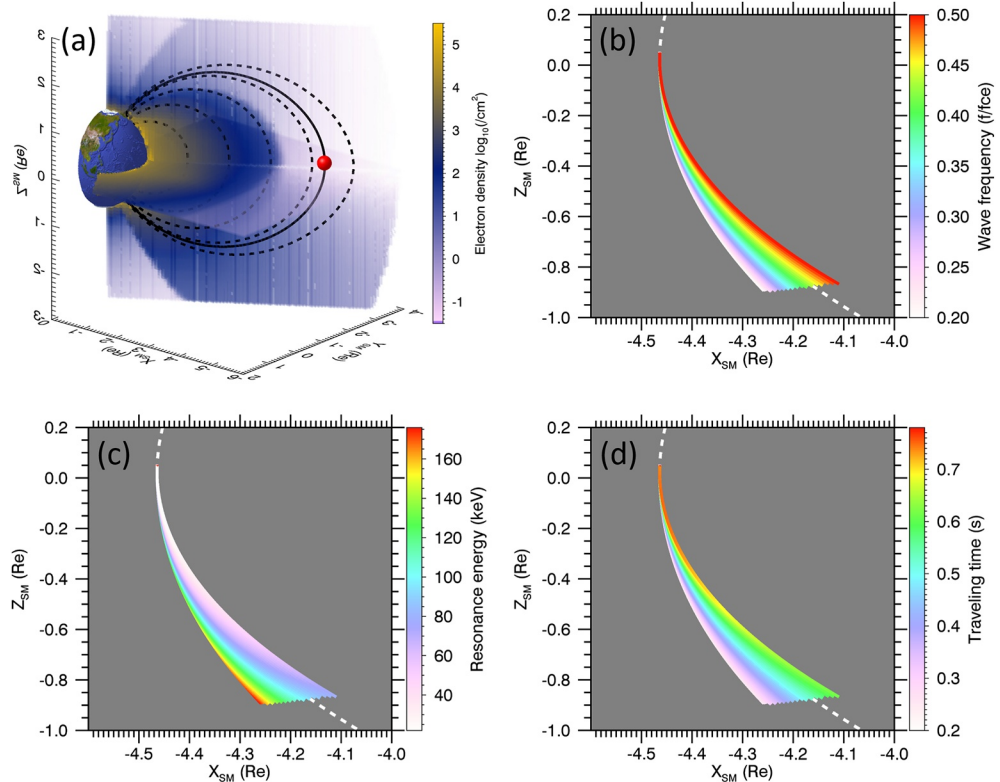
Figure 5. (a) Three-dimensional model of electron density in solar magnetic coordinates. Spatial distributions in the XZ plane of (b) spreading chorus rays, (c) resonance energy, and (d) travel time of resonant electrons to the ionosphere. The solid line in panel (a) and white dotted lines in panels (b, c, and d) indicate the geomagnetic field line connected to the point source.

keV electrons is due to the gradient in the refractive index, and drives the expansion of flash aurora primarily toward lower latitudes. The refractive index is roughly constant in the longitudinal direction due to the weak gradients of the electron density and geomagnetic field intensity, so the spatial extent in the east-west direction spreads isotropically.

Figure 6 shows the spatiotemporal evolution of the calculated VER and column emission clearly reproduces the morphological characteristics of the observed flash auroras such as predominant southward (lower-latitude side) expansion (see Movies S1 and Movie S2 in Supporting Information (SI)). The duration of the calculated VER was 0.30 s, which is similar to the observed duration of the flash auroras (see Figure 1b). We also see a time delay of the calculated VER depending on the energy (see Figure 5c and 5d). This is the same phenomenon as that of the time-of-flight effects on typical pulsating auroras (e.g., Miyoshi et al., 2010), where a travel time of 0 s is equivalent to the injected time of chorus rays. In the expansion phase, the highest-energy electrons interacting with the lowest-frequency waves at higher latitudes initially reach the upper ionosphere, and then energetic electrons interacting with waves of gradually increasing frequency at the frequency sweep rate arrive late in the ionosphere (see Figure 5). The expansion time can be characterized by the frequency sweep rate of a chorus element. In the contraction phase (0.775 s in Figure 6), the lowest-energy electrons interacting with the highest-frequency waves at the equator (of the minimum geomagnetic field) are the last to reach the ionosphere. The contraction time should be characterized by the lowest-electron energy at the equator, and thus the final contraction location in the ionosphere is related to the chorus source scale in the magnetosphere for the minimum resonance energy. Moreover, the altitude of the luminous layer varies with time depending on the precipitating electron energy. The initial luminous layer is quite narrow, in the altitude range from 95 to 100 km, and gradually extends to the range from 95 to 110 km (more easily seen from the frontal view in Figure 6b and Movie S2 in SI). These altitude variations that depend on the precipitating electron energy go beyond the scope of this study and will be
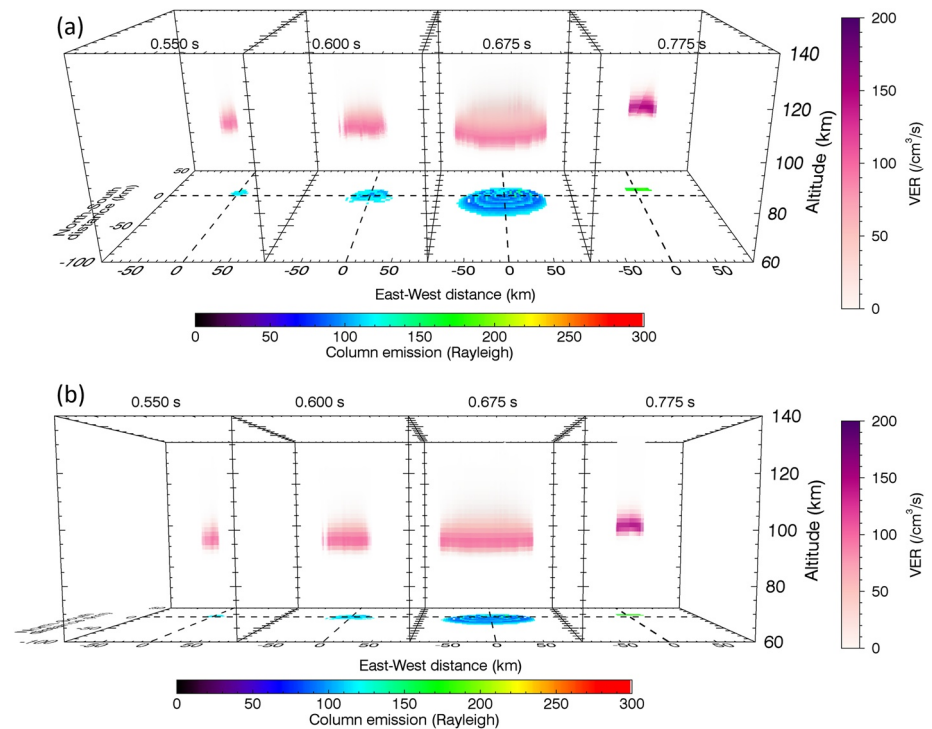
Figure 6. Four-dimensional evolution of the calculated volume emission rate (VER) and column emission at the footprints in the ionosphere connected to the wave-particle interaction region. (a) VER viewed diagonally. (b) VER viewed from the front.

part of future work using multiple high-speed EMCCD cameras. Nevertheless, this study supports earlier studies that found pulsating auroras have a narrower luminous layer in comparison with other auroral phenomena (Brown et al., 1976; Kataoka et al., 2013). To validate the vertical thickness and height of aurora based on our model calculation of spatial extent of flash aurora, we will combine both auroral tomography techniques for three-dimensional optical structures (Tanaka et al., 2011) and estimation techniques about characteristic energies using optical emissions (Aryal et al., 2018; Grubbs et al., 2018), in future studies. Our calculations can be used to resolve this long-standing issue about the vertical thickness of pulsating auroras, because our model can estimate both four-dimensional (three-dimensional space and time) auroral evolutions and characteristic energy based on the cyclotron resonance with chorus wave propagation.
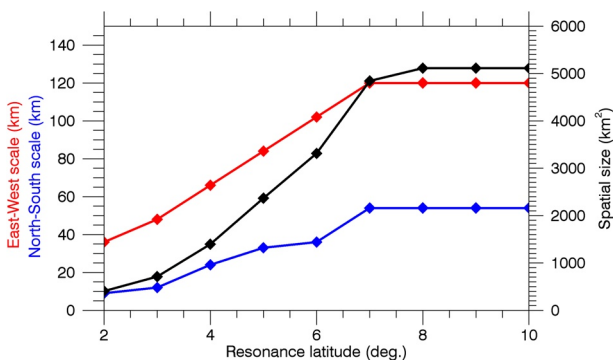
Figure 7. Spatial scale of calculated column emission in the ionosphere as a function of resonant latitude (magnetic latitude). The red and blue lines indicate the east-west and north-south scale in unit of km, respectively. The black line indicates the spatial size in unit of km².

Finally, the effects of the resonant latitude range on the spatial extent of column emission are evaluated in Figure 7. The column emission from the ground view was calculated by integrating the VER along the line of sight. The calculated column emission shows that the spatial scale in the east-west diction (red line) is larger than that for the north-south direction (blue line) as was the case with the observed flash auroras. Within the range of 2°–10°, the spatial extent of column emission increases with increasing resonant latitude until 7°, and then plateaus. This is due to the higher resonant energy interacting with chorus rays at higher latitudes not contributing to visible auroral emission. The observed spatial scales of flash aurora in the east-west and north-south directions (Figure 1a) were ~100 and 55 km, respectively. The average spatial size of flash auroras was 1,127 km² (see Figure 2c). The resonant latitude range estimated based on the average of the spatial scale of flash auroras is 4°–5°, consistent with previous statistical analyses of chorus waves (e.g., Li et al., 2009; Santolík et al., 2003; Tsurutani & Smith, 1974). This implies that chorus waves characterize not only the temporal variations of

electron precipitation, such as quasi-periodic pulsations and fast luminous modulations of pulsating auroras (Miyoshi, Saito, et al., 2015), prompt visible bursts of flash auroras, and microbursts of relativistic electrons, but also spatial variations in auroral morphology such as the predominant expansion direction.

5. Discussion and Conclusions

Although wide (tens to thousands of kilometers) transverse scales of the chorus source region deduced from multiple satellite observations of chorus elements and pulsating auroral patches have been reported in previous studies, these studies did not find the spatial asymmetry of wave-particle interaction regions due to an insufficient spatial or temporal resolution. In this study, we found that flash auroras at subauroral latitudes show strong asymmetry in terms of their spatial characteristics. The asymmetric spatial displacements were predominantly toward the southward (equatorward) extent in the ionosphere. This was found to be related to the chorus wave propagation effects in the inner magnetosphere.

Pulsating auroras have various morphological structures (e.g., Royrvik & Davis, 1977). Our calculation of the VER combined with chorus-ray tracing revealed reproducible expansion and contraction of an auroral patchy structure. From the effects of spreading chorus rays, the spatial scales of flash auroras and the wave-particle interaction regions depend on the latitude range of cyclotron resonance and the WNA distribution. The chorus wave amplitude increases as the wave propagates along the field line (Katoh & Omura, 2013). Therefore, the spatial scales of flash auroras are indirectly related to the chorus wave amplitude, consistent with earlier studies that reported that the observed auroral patch expansion is related to chorus amplitude variations (Ozaki et al., 2019). The difference in the spatial scale of pulsating auroral patches between auroral and subauroral latitudes was reported by Nishimura et al. (2011) and Ozaki et al. (2018). This difference can be explained by the difference in the expansion of chorus ray paths, because for a given initial WNA distribution and latitude range of the resonance location, the spatial extent of chorus ray paths is more spread at auroral latitudes due to the longer propagation along the field line. The key findings of this study are summarized as follows.

1. The observed flash-type auroral patches exhibit preferential southward (equatorward) expansion and contraction (cf., Figures 1a and 3).
2. The spreading chorus-ray paths could produce this equatorward preference of the auroral patch displacement at subauroral latitudes, because of the dominant earthward propagation due to the refractive index of the inner magnetosphere (cf., Figure 5).
3. The initial luminous location of a flash aurora coincides with the resonance location with the maximum energy in the magnetosphere at the high latitudes. The final luminous location of a flash aurora coincides with the equatorial resonance location with the minimum energy in the magnetosphere (cf., Figure 5).
4. The calculated column emission shows a correlation with the magnetic latitude of the resonance region at magnetic latitudes within 10° from the equatorial plane of the magnetosphere (cf., Figure 7). This correlation supports a relationship between the spatial scale of auroral patches and chorus amplitudes growing during wave propagation to higher latitudes along the field line.

The present study shows that chorus waves determine not only various temporal characteristics of precipitation electrons, but also the morphological characteristics for expansion-type auroral patches. These findings should be important for understanding the prompt developments of auroral morphology.

Data Availability Statement

The EMCCD image data used in this study are available from the ERG Science Center (http://ergsc.isee.nagoya-u.ac.jp/data_info/ground.shtml.en) (Miyoshi et al., 2018). The VER calculation is available from http://polaris.nipr.ac.jp/~aurora/eltrans/html/gtvolemi_e.html. The ray tracing code is available from http://waves.is.t.kanazawa-u.ac.jp/. The Kp index used in this study was provided by the World Data Center for Geomagnetism, Kyoto (http://wdc.kugi.kyoto-u.ac.jp/wdc/Sec3.html).

References

Agapitov, O., Blum, L. W., Mozer, F. S., Bonnell, J. W., & Wygant, J. (2017). Chorus whistler wave source scales as determined from multi-point Van Allen Probe measurements. *Geophysical Research Letters*, *44*, 2634–2642. https://doi.org/10.1002/2017GL072701

Agapitov, O., Krasnoselskikh, V., Zaliznyak, Y., Angelopoulos, V., Le Contel, O., & Rolland, G. (2010). Chorus source region localization in the Earth's outer magnetosphere using THEMIS measurements. *Annales Geophysicae*, *28*(6), 1377–1386. https://doi.org/10.5194/angeo-28-1377-2010

Albert, J. M. (2005). Evaluation of quasi-linear diffusion coefficients for whistler mode waves in a plasma with arbitrary density ratio. *Journal of Geophysical Research*, *110*, A03218. https://doi.org/10.1029/2004JA010844

Aryal, S., Finn, S. C., Hewawasam, K., Maguire, R., Geddes, G., Cook, T., et al. (2018). Derivation of the energy and flux morphology in an aurora observed at midlatitude using multispectral imaging. *Journal of Geophysical Research: Space Physics*, *123*, 4257–4271. https://doi.org/10.1029/2018JA025229

Bingham, S. T., Mouikis, C. G., Kistler, L. M., Boyd, A. J., Paulson, K., Farrugia, C. J., et al. (2018). The outer radiation belt response to the storm time development of seed electrons and chorus wave activity during CME and CIR driven storms. *Journal of Geophysical Research: Space Physics*, *123*, 10139–10157. https://doi.org/10.1029/2018JA025963

Bortnik, J., Inan, U. S., & Bell, T. F. (2006). Temporal signatures of radiation belt electron precipitation induced by lightning-generated MR whistler waves: 1. Methodology. *Journal of Geophysical Research*, *111*, A02204. https://doi.org/10.1029/2005JA011182

Breneman, A. W., Crew, A., Sample, J., Klumpar, D., Johnson, A., Agapitov, O., et al. (2017). Observations directly linking relativistic electron microbursts to whistler mode chorus: Van Allen Probes and FIREBIRD II. *Geophysical Research Letters*, *44*, 11265–11272. https://doi.org/10.1002/2017GL075001

Brown, N. B., Davis, T. N., Hallinan, T. J., & Stenbaek-Nielsen, H. C. (1976). Altitude of pulsating aurora determined by a new instrumental technique. *Geophysical Research Letters*, *3*, 403–404. https://doi.org/10.1029/GL003i007p00403

Burton, R. K., & Holzer, R. E. (1974). The origin and propagation of chorus in the outer magnetosphere. *Journal of Geophysical Research*, *79*(7), 1014–1023. https://doi.org/10.1029/JA079i007p01014

Chamberlain, J. W. (1961). *Physics of the aurora and airglow*. New York. Academic Press.

Chen, L., Thorne, R. M., Li, W., & Bortnik, J. (2013). Modeling the wave normal distribution of chorus waves. *Journal of Geophysical Research: Space Physics*, *118*, 1074–1088. https://doi.org/10.1029/2012JA018343

Chum, J., & Santolík, O. (2005). Propagation of whistler-mode chorus to low altitudes: Divergent ray trajectories and ground accessibility. *Annales Geophysicae*, *23*, 3727–3738. https://doi.org/10.5194/angeo-23-3727-2005

Coroniti, F. V., Scarf, F. L., Kennel, C. F., Kurth, W. S., & Gurnett, D. A. (1980). Detection of Jovian whistler mode chorus; Implications for the Io torus aurora. *Geophysical Research Letters*, *7*, 45–48. https://doi.org/10.1029/GL007i001p00045

Donovan, E. F., Mende, S., Jackel, B., Frey, H., Syrjäsuo, M., Voronkov, I., et al. (2006). The THEMIS all-sky imaging array—System design and initial results from the prototype imager. *Journal of Atmospheric and Terrestrial Physics*, *68*, 1472–1487. https://doi.org/10.1016/j.jastp.2005.03.027

Foster, J. C., Erickson, P. J., Omura, Y., Baker, D. N., Kletzing, C. A., & Claudepierre, S. G. (2017). Van Allen Probes observations of prompt MeV radiation belt electron acceleration in nonlinear interactions with VLF chorus. *Journal of Geophysical Research: Space Physics*, *122*, 324–339. https://doi.org/10.1002/2016JA023429

Gallagher, D. L., Craven, P. D., & Comfort, R. H. (2000). Global core plasma model. *Journal of Geophysical Research*, *105*(A8), 18819–18833. https://doi.org/10.1029/1999JA000241

Ginet, G. P., O'Brien, T. P., Huston, S. L., Johnston, W. R., Guild, T. B., Friedel, R., et al. (2013). AE9, AP9 and SPM: New models for specifying the trapped energetic particle and space plasma environment. *Space Science Reviews*, *179*(1–4), 579–615. https://doi.org/10.1007/978-1-4899-7433-4_18

Grubbs, G., II, Michell, R., Samara, M., Hampton, D., & Jahn, J.-M. (2018). Predicting electron population characteristics in 2-D using multispectral ground-based imaging. *Geophysical Research Letters*, *44*, 15–20. https://doi.org/10.1002/2017GL075873

Hanna, P. B., & Anger, C. D. (1971). Auroral colour variations, *Planetary and Space Science*, *19*, 399–411. https://doi.org/10.1016/0032-0633(71)90046-8

Horne, R. B., Glauert, S. A., & Thorne, R. M. (2003). Resonant diffusion of radiation belt electrons by whistler-mode chorus. *Geophysical Research Letters*, *30*(9), 1493. https://doi.org/10.1029/2003GL016963

Jordanova, V. K., Tu, W., Chen, Y., Morley, S. K., Panaitescu, A.-D., Reeves, G. D., & Kletzing, C. A. (2016). RAM-SCB simulations of electron transport and plasma wave scattering during the October 2012 "double-dip" storm. *Journal of Geophysical Research: Space Physics*, *121*, 8712–8727. https://doi.org/10.1002/2016JA022470

Kasahara, S., Miyoshi, Y., Kurita, S., Yokota, S., Keika, K., Hori, T., et al. (2019). Strong diffusion of energetic electrons by equatorial chorus waves in the midnight-to-dawn sector. *Geophysical Research Letters*, *46*, 12685–12692. https://doi.org/10.1029/2019GL085499

Kataoka, R., Miyoshi, Y., Hampton, D., Ishii, T., & Kozako, H. (2012). Pulsating aurora beyond the ultra-low-frequency range. *Journal of Geophysical Research*, *117*, A08336. https://doi.org/10.1029/2012JA017987

Kataoka, R., Miyoshi, Y., Shigematsu, K., Hampton, D., Mori, Y., Kubo, T., et al. (2013). Stereoscopic determination of all-sky altitude map of aurora using two ground-based Nikon DSLR cameras. *Annales Geophysicae*, *31*, 1543–1548. https://doi.org/10.5194/angeo-31-1543-2013

Katoh, Y., & Omura, Y. (2013). Effect of the background magnetic field inhomogeneity on generation processes of whistler-mode chorus and broadband hiss-like emissions. *Journal of Geophysical Research: Space Physics*, *118*, 4189–4198. https://doi.org/10.1002/jgra.50395

Kennel, C. F. (1969). Consequence of a magnetospheric plasma. *Reviews of Geophysics*, *7*(1), 379. https://doi.org/10.1029/RG007i001p00379

Kennel, C. F., & Petschek, H. E. (1966). Limit on stably trapped particle fluxes. *Journal of Geophysical Research*, *71*(1), 1–28. https://doi.org/10.1029/JZ071i001p00001

Kimura, I., Matsuo, T., Tsuda, M., & Yamauchi, K. (1985). Three dimensional ray tracing of whistler mode waves in a non-dipolar magnetosphere. *Journal of Geomagnetism and Geoelectricity*, *37*, 945–956. https://doi.org/10.5636/jgg.37.945

Kurth, W. S., & Gurnett, D. A. (1991). Plasma waves in planetary magnetospheres. *Journal of Geophysical Research*, *96*(S01), 18977–18991. https://doi.org/10.1029/91JA01819

Li, W., Ni, B., Thorne, R. M., Bortnik, J., Green, J. C., Kletzing, C. A., et al. (2013). Constructing the global distribution of chorus wave intensity using measurements of electrons by the POES satellites and waves by the Van Allen Probes. *Geophysical Research Letters*, *40*, 4526–4532. https://doi.org/10.1002/grl.50920

Li, W., Thorne, R. M., Angelopoulos, V., Bortnik, J., Cully, C. M., Ni, B., et al. (2009). Global distribution of whistler-mode chorus waves observed on the THEMIS spacecraft. *Geophysical Research Letters*, *36*, L09104. https://doi.org/10.1029/2009GL037595

Li, W., Thorne, R. M., Ma, Q., Ni, B., Bortnik, J., Baker, D. N., et al. (2014). Radiation belt electron acceleration by chorus waves during the 17 March 2013 storm. *Journal of Geophysical Research: Space Physics*, *119*, 4681–4693. https://doi.org/10.1002/2014JA019945

Lorentzen, K. R., Blake, J. B., Inan, U. S., & Bortnik, J. (2001). Observations of relativistic electron microbursts in association with VLF chorus. *Journal of Geophysical Research*, *106*(A4), 6017–6027. https://doi.org/10.1029/2000JA003018

Ma, Q., Li, W., Bortnik, J., Thorne, R. M., Chu, X., Ozeke, L. G., et al. (2018). Quantitative evaluation of radial diffusion and local acceleration processes during GEM challenge events. *Journal of Geophysical Research: Space Physics*, *123*, 1938–1952. https://doi.org/10.1002/2017JA025114

Malkov, M. A., Diamond, P. H., & Sagdeev, R. Z. (2011). Mechanism for spectral break in cosmic ray protonspectrum of supernova remnant W44. *Nature Communications*, *2*, 194. https://doi.org/10.1038/ncomms1195

Menietti, J. D., Schippers, P., Katoh, Y., Leisner, J. S., Hospodarsky, G. B., Gurnett, D. A., & Santolik, O. (2013). Saturn chorus intensity variations. *Journal of Geophysical Research: Space Physics*, *118*, 5592–5602. https://doi.org/10.1002/jgra.50529

Miyoshi, Y., Hori, T., Shoji, M., Teramoto, M., Chang, T. F., Segawa, T., et al. (2018). The ERG Science Center. *Earth Planets and Space*, *70*, 96. https://doi.org/10.1186/s40623-018-0867-8

Miyoshi, Y., Kataoka, R., Kasahara, Y., Kumamoto, A., Nagai, T., & Thomsen, M. (2013). High-speed solar wind with southward interplanetary magnetic field causes relativistic electron flux enhancement of the outer radiation belt via enhanced condition of whistler waves. *Geophysical Research Letters*, *40*, 4520–4525. https://doi.org/10.1002/grl.50916

Miyoshi, Y., Katoh, Y., Nishiyama, T., Sakanoi, T., Asamura, K., & Hirahara, M. (2010). Time of flight analysis of pulsating aurora electrons, considering wave-particle interactions with propagating whistler mode waves. *Journal of Geophysical Research*, *115*, A10312. https://doi.org/10.1029/2009JA015127

Miyoshi, Y., Morioka, A., Obara, T., Misawa, H., Nagai, T., & Kasahara, Y. (2003). Rebuilding process of the outer radiation belt during the November 3, 1993, magnetic storm—NOAA and EXOS-D observations. *Journal of Geophysical Research*, *108*(A1), 1004. https://doi.org/10.1029/2001JA007542

Miyoshi, Y., Oyama, S., Saito, S., Fujiwara, H., Kataoka, R., Ebihara, Y., et al. (2015). Energetic electron precipitation associated with pulsating aurora: EISCAT and Van Allen Probes observations. *Journal of Geophysical Research: Space Physics*, *120*, 2754–2766. https://doi.org/10.1002/2014JA020690

Miyoshi, Y., Saito, S., Kurita, S., Asamura, K., Hosokawa, K., Sakanoi, T., et al. (2020). Relativistic electron microbursts as high-energy tail of pulsating aurora electrons. *Geophysical Research Letters*, *47*, e2020GL090360. https://doi.org/10.1029/2020GL090360

Miyoshi, Y., Saito, S., Seki, K., Nishiyama, T., Kataoka, R., Asamura, K., et al. (2015). Relation between energy spectra of pulsating aurora electrons and frequency spectra of whistler-mode chorus waves. *Journal of Geophysical Research: Space Physics*, *120*, 7728–7736. https://doi.org/10.1002/2015JA021562

Mozer, F. S., Agapitov, O. V., Blake, J. B., & Vasko, I. Y. (2018). Simultaneous observations of lower band chorus emissions at the equator and microburst precipitating electrons in the ionosphere. *Geophysical Research Letters*, *45*, 511–516. https://doi.org/10.1002/2017GL076120

Ni, B., Thorne, R. M., Shprits, Y. Y., & Bortnik, J. (2008). Resonant scattering of plasma sheet electrons by whistler-mode chorus: Contribution to diffuse auroral precipitation. *Geophysical Research Letters*, *35*, L11106. https://doi.org/10.1029/2008GL034032

Nishimura, Y., Bortnik, J., Li, W., Thorne, R. M., Chen, L., Lyons, L. R., et al. (2011). Multievent study of the correlation between pulsating aurora and whistler mode chorus emissions. *Journal of Geophysical Research*, *116*, A11221. https://doi.org/10.1029/2011JA016876

Nishimura, Y., Lessard, M. R., Katoh, Y., Miyoshi, Y., Grono, E., Partamies, N., et al. (2020). Diffuse and pulsating aurora. *Space Science Reviews*, *216*, 4. https://doi.org/10.1007/s11214-019-0629-3

Ogawa, Y., Tanaka, Y., Kadokura, A., Hosokawa, K., Ebihara, Y., Motoba, T., et al. (2020). Development of low-cost multi-wavelength imager system for studies of aurora and airglow. *Polar Science*, *23*, 100501. https://doi.org/10.1016/j.polar.2019.100501

Oguchi, T. (1978). Observations of rapid auroral fluctuations. *Journal of Geomagnetism and Geoelectricity*, *30*(4), 299–314. https://doi.org/10.5636/jgg.30.299

Omura, Y., Furuya, N., & Summers, D. (2007). Relativistic turning acceleration of resonant electrons by coherent whistler mode waves in a dipole magnetic field. *Journal of Geophysical Research*, *112*, A06236. https://doi.org/10.1029/2006JA012243

Omura, Y., Miyashita, Y., Yoshikawa, M., Summers, D., Hikishima, M., Ebihara, Y., & Kubota, Y. (2015). Formation process of relativistic electron flux through interaction with chorus emissions in the Earth's inner magnetosphere. *Journal of Geophysical Research: Space Physics*, *120*, 9545–9562. https://doi.org/10.1002/2015JA021563

Ono, T. (1993). Derivation of energy parameters of precipitating auroral electrons by using the intensity ratios of auroral emissions. *Journal of Geomagnetism and Geoelectricity*, *45*(6), 455–472. https://doi.org/10.5636/jgg.45.455

Otsu, N. (1979). A threshold selection method from gray-level histograms. *IEEE Transactions on Systems, Man, and Cybernetics*, *9*(1), 62–66. https://doi.org/10.1109/TSMC.1979.4310076

Ozaki, M., Miyoshi, Y., Shiokawa, K., Hosokawa, K., Oyama, S.-I., Kataoka, R., et al. (2019). Visualization of rapid electron precipitation via chorus element wave–particle interactions. *Nature Communications*, *10*, 257. https://doi.org/10.1038/s41467-018-07996-z

Ozaki, M., Shiokawa, K., Miyoshi, Y., Hosokawa, K., Oyama, S., Yagitani, S., et al. (2018). Microscopic observations of pulsating aurora associated with chorus element structures: Coordinated Arase satellite-PWING observations. *Geophysical Research Letters*, *45*, 12125–12134. https://doi.org/10.1029/2018GL079812

Rosenberg, T. J., Siren, J. C., Matthews, D. L., Marthinsen, K., Holtet, J. A., Egeland, A., et al. (1981). Conjugacy of electron microbursts and VLF chorus. *Journal of Geophysical Research*, *86*(A7), 5819–5832. https://doi.org/10.1029/JA086iA07p05819

Royrvik, O., & Davis, T. N. (1977). Pulsating aurora: Local and global morphology. *Journal of Geophysical Research*, *82*(29), 4720–4740. https://doi.org/10.1029/JA082i029p04720

Sagdeev, R. Z., Shapiro, V. D., Shevchenko, V. I., & Szego, K. (1986). MHD turbulence in the solar wind-comet interaction region. *Geophysical Research Letters*, *13*(2), 85–88. https://doi.org/10.1029/GL013i002p00085

Santolík, O., & Gurnett, D. A. (2003). Transverse dimensions of chorus in the source region. *Geophysical Research Letters*, *30*(2), 1031. https://doi.org/10.1029/2002GL016178

Santolík, O., Gurnett, D. A., Pickett, J. S., Parrot, M., & Cornilleau-Wehrlin, N. (2003). Spatio-temporal structure of storm-time chorus. *Journal of Geophysical Research*, *108*, 1278. https://doi.org/10.1029/2002JA009791

Seki, K., Miyoshi, Y., Ebihara, Y., Katoh, Y., Amano, T., Saito, S., et al. (2018). Theory, modeling, and integrated studies in the Arase (ERG) project. *Earth Planets and Space*, *70*, 17. https://doi.org/10.1186/s40623-018-0785-9

Shen, X.-C., Li, W., Ma, Q., Agapitov, O., & Nishimura, Y. (2019). Statistical analysis of transverse size of lower band chorus waves using simultaneous multisatellite observations. *Geophysical Research Letters*, *46*, 5725–5734. https://doi.org/10.1029/2019GL083118

Shiokawa, K., Katoh, Y., Hamaguchi, Y., Yamamoto, Y., Adachi, T., Ozaki, M., et al. (2017). Ground-based instruments of the PWING project to investigate dynamics of the inner magnetosphere at subauroral latitudes as a part of the ERG-ground coordinated observation network. *Earth Planets and Space*, *69*(1), 160. https://doi.org/10.1186/s40623-017-0745-9

Shiokawa, K., Katoh, Y., Satoh, M., Ejiri, M. K., Ogawa, T., Nakamura, T., et al. (1999). Development of optical mesosphere thermosphere imagers (OMTI). *Earth Planets and Space*, *51*, 887–896. https://doi.org/10.1186/bf03353247

Soria-Santacruz Pich, M., Jun, I., & Evans, R. (2017). Empirical radiation belt models: Comparison with in situ data and implications for environment definition. *Space Weather*, *15*, 1165–1176. https://doi.org/10.1002/2017SW001612

Summers, D., Omura, Y., Miyashita, Y., & Lee, D.-H. (2012). Nonlinear spatiotemporal evolution of whistler mode chorus waves in Earth's inner magnetosphere. *Journal of Geophysical Research*, *117*, A09206. https://doi.org/10.1029/2012JA017842

Summers, D., Thorne, R. M., & Xiao, F. (1998). Relativistic theory of wave-particle resonant diffusion with application to electron acceleration in the magnetosphere. *Journal of Geophysical Research*, *103*(A9), 20487–20500. https://doi.org/10.1029/98JA01740

Tanaka, Y.-M., Aso, T., Gustavsson, B., Tanabe, K., Ogawa, Y., Kadokura, A., et al. (2011). Feasibility study on generalized-aurora computed tomography. *Annales Geophysicae*, *29*, 551–562. https://doi.org/10.5194/angeo-29-551-2011

Tao, X., Bortnik, J., Albert, J. M., & Thorne, R. M. (2012). Comparison of bounce-averaged quasi-linear diffusion coefficients for parallel propagating whistler mode waves with test particle simulations. *Journal of Geophysical Research*, *117*, A10205. https://doi.org/10.1029/2012JA017931

Teng, S., Tao, X., Xie, Y., Zonca, F., Chen, L., Fang, W. B., & Wang, S. (2017). Analysis of the duration of rising tone chorus elements. *Geophysical Research Letters*, *44*, 12074–12082. https://doi.org/10.1002/2017GL075824

Thorne, R. M., Li, W., Ni, B., Ma, Q., Bortnik, J., Chen, L., et al. (2013). Rapid local acceleration of relativistic radiation belt electrons by magnetospheric chorus. *Nature*, *504*(7480), 411–414. https://doi.org/10.1038/nature12889

Thorne, R. M., Ni, B., Tao, X., Horne, R. B., & Meredith, N. P. (2010). Scattering by chorus waves as the dominant cause of diffuse auroral precipitation. *Nature*, *467*(7318), 943–946. https://doi.org/10.1038/nature09467

Treumann, R. A. (2006). The electron–cyclotron maser for astrophysical application. *Astronomy and Astrophysics Review*, *13*(4), 229–315. https://doi.org/10.1007/s00159-006-0001-y

Tsurutani, B. T., & Smith, E. J. (1974). Postmidnight chorus: A substorm phenomenon. *Journal of Geophysical Research*, *79*(1), 118–127. https://doi.org/10.1029/JA079i001p00118

Tsyganenko, N. A. (2002). A model of the near magnetosphere with a dawn-dusk asymmetry: 1. Mathematical structure. *Journal of Geophysical Research*, *107*(A8), 1179. https://doi.org/10.1029/2001JA000219

Turner, D. L., Lee, J. H., Claudepierre, S. G., Fennell, J. F., Blake, J. B., Jaynes, A. N., et al. (2017). Examining coherency scales, substructure, and propagation of whistler mode chorus elements with Magnetospheric Multiscale (MMS). *Journal of Geophysical Research: Space Physics*, *122*, 11201–11226. https://doi.org/10.1002/2017JA024474

Winske, D., & Leroy, M. M. (1984). Diffuse ions produced by electromagnetic ion beam instabilities. *Journal of Geophysical Research*, *89*(A5), 2673–2688. https://doi.org/10.1029/JA089iA05p02673